CrossMark

# Effect of Applied Potential on Fatigue Life of Electropolished Nitinol Wires

Shiril Sivan[1,2] · Matthew Di Prima[1] · Jason D. Weaver[1]

**Abstract** Nitinol is used as a metallic biomaterial in medical devices due to its shape memory and pseudoelastic properties. The clinical performance of nitinol depends on factors which include the surface finish, the local environment, and the mechanical loads to which the device is subjected. Preclinical evaluations of device durability are performed with fatigue tests while electrochemical characterization methods such as ASTM F2129 are employed to evaluate corrosion susceptibility by determining the rest potential and breakdown potential. However, it is well established that the rest potential of a metal surface can vary with the local environment. Very little is known regarding the influence of voltage on fatigue life of nitinol. In this study, we developed a fatigue testing method in which an electrochemical system was integrated with a rotary bend wire fatigue tester. Samples were fatigued at various strain levels at electropotentials anodic and cathodic to the rest potential to determine if it could influence fatigue life. Wires at potentials negative to the rest potential had a significantly higher number of cycles to fracture than wires held at potentials above the breakdown potential. For wires for which no potential was applied, they had fatigue life similar to wires at negative potentials.

✉ Jason D. Weaver
  jason.weaver@fda.hhs.gov

  Shiril Sivan
  shiril.sivan@fda.hhs.gov

1 Division of Applied Mechanics, Office of Science and Engineering Laboratories, Center for Devices and Radiological Health, U.S. Food and Drug Administration, Silver Spring, MD 20993, USA

2 Oak Ridge Institute for Science and Education, Oak Ridge, TN, USA

**Keywords** Nitinol · Fatigue · Fracture

## Introduction

Nitinol is a commonly used metal alloy in implantable cardiovascular devices such as peripheral stents in large part due to its pseudoelastic properties [1]. Despite these devices showing excellent durability during in vitro studies, some peripheral stents and aortic endografts have been reported to have fractured in vivo [2, 3]. Although factors such as mechanical fatigue, increased shear stresses at the implantation site, strut damage from fretting in the overlapped stents are some of the major mechanisms [3] that caused stent fracture, the local physiochemical environment can also play a role. Most of the in vitro tests fail to mimic these clinical scenarios because of complex in vivo implant–tissue interactions. The in vivo environment is difficult to replicate because the biomechanics of the tissue–implant interface evolves over time as the device integrates with the body. The local environment can influence the rest potential of the implant and this can impact its corrosion susceptibility. Often on implantation of a device, a foreign body reaction is initiated by the cells of the immune system where inflammatory cells can alter the local environment by reducing the pH [4]. This change in pH could influence the integrity of the oxide layer and lead to its breakdown [5]. This can cause the metal's rest potential to change to a more positive potential. Whereas, in a configuration of overlapping stents where fretting could occur, the overall electropotential can undergo a negative shift [6].

There are other instances where the potential of the metal surface can play a crucial role in the durability of the device. Recent reports of failure of insulation on wire leads used in implantable cardioverter defibrillators (ICD) and

pacemakers have resulted in externalization of the metal wires and may also result in higher strains in wire leads [7]. Leads with damaged insulations may continue to function for months before they fail and present a clinical indication [8]. Although most of the wires in leads are double insulated, damage of the second layer of insulation has been reported [9, 10]. This would expose the active metal wire to the local physiological environment and cause the metal surface's electropotential to deviate from its rest potential during its pacing activities. Although uncommon, this can result in active corrosion of the exposed wires and in some cases cause electric arcing between the wires and the generator casing [9, 11]. In some cases, the wires might experience higher strains as a result of the externalization [12].

The electropotential of a metal surface can vary and depends on the local environment. However, very little is known regarding the open circuit potentials of cardiovascular devices in vivo and how an applied electropotential may impact the integrity of the device. Numerous studies have shown that the corrosion resistance of a metal surface can change when it is immersed in an environment that mimics an inflammatory reaction. Specifically, it was shown that the open circuit potential of the metal surface can become more positive and vary with time when immersed in Phosphate Buffered Saline (PBS) having hydrogen peroxide and other acids when compared to those measured in just PBS [13–15]. A recent study by Lonn et al. [16] reported on how the open circuit potential (OCP) of nitinol can vary with or without aeration of PBS. The chemistry of the surface oxide and the duration of immersion in the test solution were also shown to influence the OCP of nitinol. Specifically, Lonn found the OCP of electropolished nitinol was the lowest when it was measured in vivo ($-400 \pm 27$ mV vs. SCE) and in in vitro blood ($-387 \pm 21$ mV vs. SCE) and OCP was more positive when nitinol was immersed in aerated PBS ($-255 \pm 61$ mV vs. SCE). Other factors such as the presence of proteins [17] and type of surface treatments [18] and mechanical fatigue [19] are also known to influence the rest potential of the metal surface. However, very little is known regarding how the rest potential of these devices would evolve over the course of implantation time.

Hence, it is important to study the effect of applied electropotential on the fatigue life of metallic wires. By enforcing the electropotential of the metal surface and subjecting the metal to cyclic fatigue, it would enable us to better predict the durability of these devices when they are subjected to mechanical stresses under inflammatory or fretting-like conditions. In this study, we combined rotary beam wire fatigue testers with potentiostats to evaluate the effect of electropotential on fatigue life. In one set of tests, the electropotential of the wires was monitored in order to determine how the rest potential of the wires would evolve when subjected to cyclic fatigue. To investigate the effect of applied potential on the fatigue life of the metal wires at a fixed alternating strain, we subjected the wires to discrete cathodic and anodic potentials while the wire underwent fatigue. We also investigated how the effect of potential would influence the fatigue life of nitinol wires when they were subjected to different levels of strain. As a characterization of our materials, we also measured their open circuit potential and breakdown potential per ASTM F2129, Standard Test Method for Conducting Cyclic Potentiodynamic Polarization Measurements to Determine the Corrosion Susceptibility of Small Implant Devices [20].

## Materials and Methods

Electropolished nitinol wires having a diameter of 0.50 mm were used for all fatigue experiments; Table 1 shows the material properties for the wire. Different levels of strain were achieved in unguided wire fatigue tests by using the following equations from ASTM E2948 [21]:

$$R = 0.417\ C$$
$$L = 2.19\ C$$

$$\varepsilon_a = \frac{\left(\frac{d}{2}\right)}{\left(\frac{R}{100}\right)},$$

where $R$ is the minimum radius, $C$ is the span between the counter rotating chucks, L is the test length of the wire, $\varepsilon_a$ is the level of alternating strain, and $d$ is the diameter of the wire.

**Table 1** Material properties for the nitinol wire

| Material characterization | |
| --- | --- |
| Upper plateau strength @ 37 °C (MPa) | 615.63 |
| Lower plateau strength @ 37 °C (MPa) | 353.44 |
| Ultimate tensile strength @ 37 °C (MPa) | 1552.33 |
| Uniform elongation @ 37 °C (%) | 10.2 |

| Transformation temperatures | |
| --- | --- |
| **Forward transformation (Cooling)** | **Reverse transformation (Heating)** |
| $R$-phase start temperature ($R_s$) = 19 °C | $R'$-phase start temperature ($R'_S$ = $-32$ °C) |
| $R$-phase finish temperature ($R_f$) = $-8$ °C | $R'$-phase finish temperature ($R'_f$ = $-5$ °C) |
| Martensite start temperature ($M_s$) $\leq -125$ °C | Austenite start temperature ($A_s$) = $-6$ °C |
| | Austenite finish temperature ($A_f$) = 19 °C |

The $M_s$ value is approximate due to equipment limitations

Fatigue life was evaluated using a rotary bend wire fatigue tester (Blockwise, Tempe, AZ) equipped with optical wire break detection. All fatigue tests were conducted at 3600 rpm with the wires submerged partially in phosphate buffered saline (PBS) (Fisher Scientific, NH). The temperature was maintained at 37 °C throughout the experiment using a Teflon-coated immersion heater (Cole Palmer, IL). To compensate for evaporative loss, the level of PBS was monitored using water level detectors and fresh deionized (DI) water was pumped into the test reservoir to maintain PBS concentration.

## Test Plan

The following test plan was used to characterize the electropolished nitinol used for this study and to study the effect of applied potential on fatigue life of electropolished nitinol wires.

- Potentiodynamic polarization testing to determine the rest-potential and breakdown potentials for the electropolished wires used for all the experiments.
- Fatigue experiments with electrochemical control:

  1. Open Circuit Potential Characterization during Wire Fatigue at 1% Alternating Strain. (Monitor the open circuit potential during wire fatigue at fixed 1% $\varepsilon_a$).
  2. Effect of Applied Potential on Fatigue Life at 1% Alternating Strain. (Determine the effect of applied potential on fatigue life at fixed 1% $\varepsilon_a$).
  3. Effect of Alternating Strain and Applied Potential on Fatigue Life. (Determine the synergistic effect of strain and applied potential on fatigue life).

- Scanning electron microscopy of the wire fracture surfaces.

## Potentiodynamic Polarization Testing

Six wire samples were cut from the same lot and mounted onto wire specimen holders using silver paint (Fast Drying Silver Paint, Ted Pella Inc., CA). The cut end of the wires and the silver-painted ends of the specimens were masked off using two coats of lacquer (MICCROStop, Tolber Chemical Division, AK). The rest of the wire specimen holder was wrapped with parafilm to assure that no part of the specimen holder came in contact with the PBS. ASTM F2129, "Standard Test Method for Conducting Cyclic Potentiodynamic Polarization Measurements to Determine the Corrosion Susceptibility of Small Implant Devices,"

was performed on these specimens in PBS. ASTM F2129 in brief, involves deaerating PBS with pure nitrogen at 150 cc/min for 30 min after which the test sample is submerged into PBS. The OCP is measured and recorded for 1 h. The OCP measured at the end of the hour was established as the rest potential ($E_r$). The voltage is then scanned potentiodynamically in the positive direction up to 1000 mV versus SCE at the rate of 1 mV/s. The breakdown potential was determined to be the potential at which the current densities rose by at least two decades. The potential is then scanned in the negative direction back to the rest potential at the same scan rate.

## Electrochemical Setup

A Model 263A (Princeton Applied Research, Oak Ridge, TN) potentiostat or an Interface 1000 (Gamry, Warminister, PA) system was used for all electrochemical procedures in this study. All potentiostats were in compliance with ASTM G5, "Standard Reference Test Method for Making Potentiodynamic Anodic Polarization Measurements." The cut portions of the wire that would go into the wire chucks on the wire fatigue testers were insulated with three coats of lacquer to prevent any transient electrical noise from the wire fatigue testers. A check for leakage of electrical noise from the instrument to the wire sample was checked before and after the end of the fatigue test by simply monitoring OCP of the specimen with all connections in place. Wire samples that failed the check for electrical noise from improper insulation for the wire ends were eliminated and were replaced with a new wire specimen. All electrochemical measurements were achieved using a three-electrode system with carbon rod acting as a counter electrode and saturated calomel electrode (SCE) as a reference electrode (Fig. 1a). Electric connectivity to the rotating wire mounted on the rotary bend wire fatigue tester was established by using a custom-made magnetic clasp made from graphite as shown in Fig. 1b.

The magnetic clasp was made by machining a groove that could hold the rotating wire onto a graphite electrode. A small hole was drilled onto the side of one half of the graphite clasp and filled with fast-drying silver paint. Scrap nitinol wires were then inserted into the hole to establish electric connectivity with the clasp. To ensure proper uninterrupted electric connection to rotating wire, the two sides of the clasp were held together by strong magnets embedded into the face of the clasp as shown in Fig. 1b. The wire in the groove could rotate freely without causing wear of the wire or the groove since the graphite was self-lubricating and at the same time provided excellent electric connectivity. Electrical connectivity between the clasp and the wire was checked by using a multimeter before and after the end of the fatigue test to assure that electrical connectivity was maintained throughout the experiment.
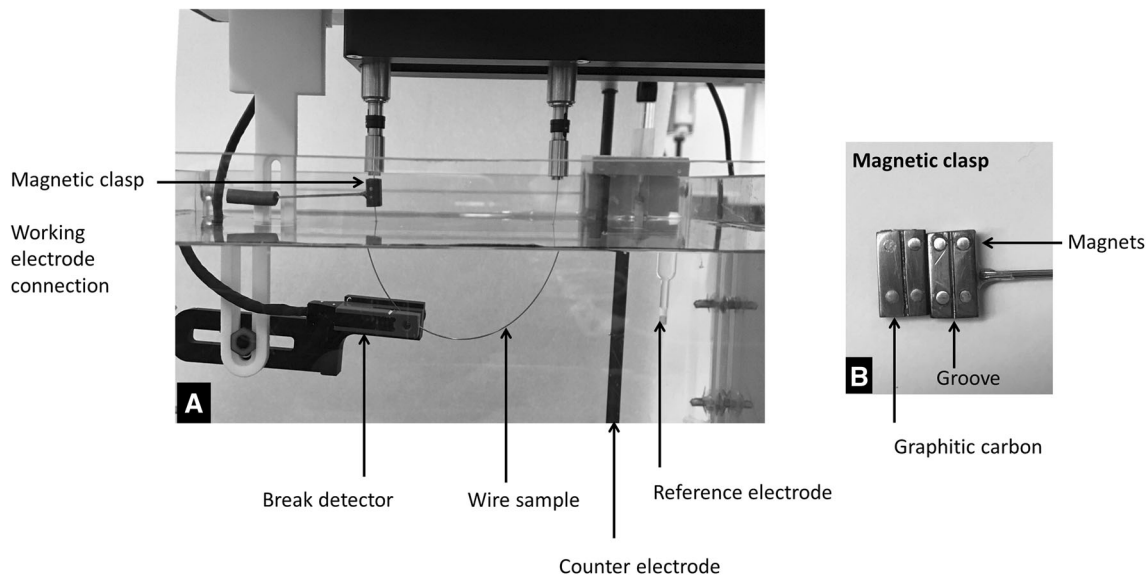
**Fig. 1** **a** The electrochemical setup integrated with the rotary bend wire fatigue machine. **b** Shows that the electrical connections to the rotating wire were established using a custom-made magnetic clasp

## Open Circuit Potential Characterization During Wire Fatigue at 1% Alternating Strain

In order to understand how the rest potential of the wire would vary while it underwent fatigue, we monitored the open circuit potential of the wire for 10 min after which we subjected the wire to an alternating strain of 1%. We then continued to monitor the OCP of the wire until fracture occurred. For one of the samples, the test was terminated once a significant drop in its OCP was observed. This sample was then rinsed with deionized water and prepared for imaging using a scanning electron microscope.

## Effect of Applied Potential on Fatigue Life at 1% Alternating Strain

To determine if an applied potential would influence the fatigue life of nitinol wires, we potentiostatically held the wire at −500 through +600 (mV vs. SCE) in increments of 100 mV. We chose an alternating strain of 1% for these experiments to represent a high alternating strain scenario and for shorter test times. The OCP was monitored for the initial 10-min soak period after which the wire was held at a discrete chosen potential within the −500 to 600 mV versus SCE range (not OCP) and the fatigue test was initiated after 10 s at the chosen potential. The current density was recorded throughout the potentiostatic step until wire fracture. All applied potentials for the potentiostatic step were enforced relative to the reference electrode and not OCP. Six wire samples were tested for every potential.

## Effect of Alternating Strain and Applied Potential on Fatigue Life

The fatigue life of the electropolished nitinol wires was evaluated at alternating strains of 1.2, 1.0, 0.8, 0.6, and 0.5%. The OCP of the wires were recorded for 10 min before the chosen potential was applied. The wires were potentiostatically held at either −400, OCP, or at +400 mV versus SCE. These potentials were chosen because −400 mV is cathodic to the breakdown potential, OCP is the rest potential and representative of how fatigue tests are typically conducted, and +400 mV versus SCE is more positive to the breakdown potential. Once the potential was applied potentiostatically to the wire, the current density was monitored for 10 s after which the fatigue test was started. We continued to monitor the current density of the wire until fracture occurred. Six wire samples were tested for all strains except for OCP at 0.5% strain for which only three samples were tested since wires did not fracture for ten million cycles and were deemed run outs.

## Scanning Electron Microscopy

A scanning electron microscope (SEM) was used to observe the fracture surface of representative samples from wires that were fatigued at low strain ($\varepsilon_a = 0.5\%$) and potentiostatically held at −400 mV versus SCE and +400 mV versus SCE. The fractured wires were cut using a wire cutter to reduce the specimen size and transferred into a centrifuge tube containing DI water where they were sonicated for 10 min. The wires were then mounted onto

specimen holders using a conductive carbon double-sided adhesive tape (Ted Pella Inc., CA). Images of the fractured surface were acquired using secondary and backscatter electron imaging modes.

## Statistical Analysis

One-way analysis of variance (ANOVA) with Tukey pairwise comparisons was performed with $\alpha = 0.05$ to determine statistical significance among groups. Wires that survived up to 10 million cycles were considered run outs. For censored data (run outs), a non-parametric distribution analysis for right censored data was used to determine if the groups were significantly different.

## Results

The results of the potentiodynamic scan from the ASTM F2129 procedure were the rest potential and breakdown potential. The average rest potential was $-74.9 \pm 16.5$ mV (vs. SCE). Five out of the six wires had a breakdown potential at $246.7 \pm 22.6$ mV versus SCE which shows that there is variability in corrosion susceptibility of the wires belonging to the same lot. The pitting corrosion resulting from electrochemical breakdown on the wires was localized and in most cases resulted in the complete disintegration of the test specimen. For the sample that did not experience a breakdown, the current response showed a distinct passive region followed by lower current densities on the reverse scan showing that there was no pitting.

While the rest potentials for wire that were not undergoing fatigue were stable around $-75$ mV, there was a characteristic negative shift in rest potential when the wire was subjected to alternating strain of 1% as shown in Fig. 2a. During the initial soak period, the OCP gradually reached an equilibrium at which the fatigue test was initiated. The OCP of the wire undergoes a sudden shift in the cathodic direction at the start of the fatigue test and gradually stabilizes to approximately $-300$ mV versus SCE which is about 200 mV negative to the rest potential at the start of the fatigue test. The OCP remains stable around $-300$ mV versus SCE for a number of cycles until there is a sudden drop to $-700$ mV versus SCE when the wire fractures. The fatigue test ends at this point and the rest potential of the wire gradually recovers in the positive direction.

Figure 2b illustrates the typical current response when a nitinol wire is potentiostatically held at a potential that was in-between its average rest potential and breakdown potential while it was subjected to fatigue. The current density initially drops off and stabilizes as soon as the wire

sample was potentiostatically held at 100 mV. At approximately 10 s into potentiostatic hold, the fatigue test is initiated. The current densities initially rise up rapidly when the fatigue test was initiated and then gradually fall and stabilize. After approximately 90 s, the current densities start to gradually rise again. The current densities are the highest when the wire fractures. Post wire fracture, the current densities rapidly drop off. Whereas, when a wire is held potentiostatically at a potential that was negative to the rest potential ($-400$ mV vs. SCE), the current densities rise anodically until it stabilizes (Fig. 2c). Similarly, when a wire is held at a potential that is above breakdown potential, the current densities stabilize for a short period after the fatigue test has started but then it starts to rise erratically (Fig. 2d). The current density remains high and continues to fluctuate even after the wire had fractured mainly because some sections of the wire continued to undergo corrosion.

Figure 3 shows the means and standard deviations for the number of cycles to failure for wires that were held at potentials in the range of $-500$ to $+600$ mV versus SCE in increments of 100 mV and subjected to alternating strains of 1%. Wires held at potentials positive to the breakdown potential failed earlier as compared to wires held at potentials lower than the rest potential. Figure 4 shows the strain- number of cycles to failure (S–N) curve for wires that were held at $+400$, $-400$ mV versus SCE and OCP. For 0.8% strain, there is a clustering of number of cycles for failure for all potentials. At 0.5% strain, wires potentiostatically held at $-400$ mV versus SCE and OCP were run outs (exceeded 10 million cycles). Whereas, wires held at $+400$ mV versus SCE failed at around 20,000 cycles. The number of cycles to failure for wires that were potentiostatically held at $+400$ mV versus SCE was significantly lower ($p < 0.05$) than $-400$ mV versus SCE for all strains. There was no significant difference in the number of cycles to failure between wires potentiostatically held at $-400$ mV and OCP for all strains except for 1.2%.

The SEM images show the fracture surfaces of the wires when held at $+400$ and $-400$ mV versus SCE and after being subjected to an alternating strain of 0.5% (Fig. 5). The white arrows on Fig. 5 point to the location for nucleation and initiation of the fatigue crack. Figure 5c in secondary and (d) in backscatter shows a high magnification image of the location (white arrow) of the initiation of the crack. The images show that the site of initiation of the crack occurred at the location of an inclusion at the surface of the wire. Whereas, wires that were held potentiostatically at $+400$ mV versus SCE, potentials anodic to the breakdown potential and at 0.5% strain had severe pitting at the site of initiation of the crack. Figure 5e in secondary and Fig. 5f in backscatter shows that the fracture surface of
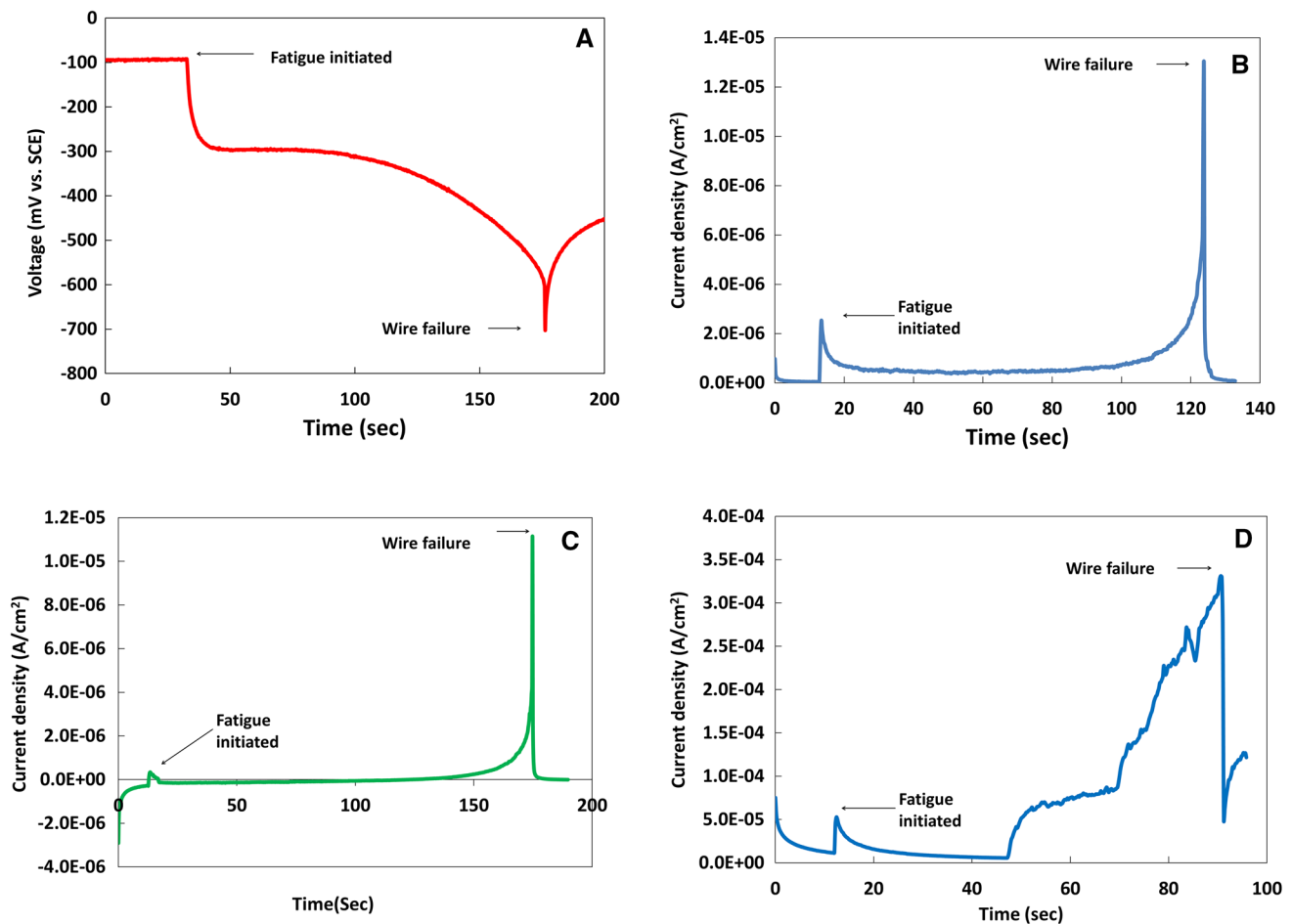
Fig. 2 a Shows a typical voltage transient observed when a nitinol wire is subjected to alternating strain of 1%. The above figure also shows the current density monitored while a wire was potentiostatically held at **b** 100 mV, **c** −400 mV, and **d** +400 mV (vs. SCE) and subjected to alternating strain of 1%

the wire had severe pitting. The SEM images, Fig. 5g, h, show that these pits had a spherical interconnected morphology and appear to radiate from nucleation point in the direction of the crack growth. The corresponding backscatter image shows that some of the pits are filled with corrosion byproducts which appear in darker gray color.

## Discussion

The results presented in this study show that the applied potential can influence the fatigue life of nitinol wires. This appears to be because active corrosion of the metal surface causes the formation of new pits which can subsequently act as sites for the nucleation of cracks. Whereas, at potentials that are negative to the rest potential, corrosion will be suppressed. Pitting did not occur on the surface of the wires at these negative potentials for the wires used in this study. This results in a larger number of cycles to failure because crack initiation and propagation arises only from the surface defects already present on the wire.

By monitoring the OCP of the wire under fatigue, we were able to understand how the electropotential of the metal surface would change as the metal was subjected to alternating strains. The rest potential of the wire can change even when there are no potentials enforced. Typically, the rest potential for passive metal surfaces would stabilize and tend to reach a value close to 0 mV [22]. While a wire is subjected to mechanical fatigue, surface defects like inclusions on the metal surface can act as stress risers which make these locations more susceptible to nucleation of cracks. As a crack grows with each alternating strain cycle, the opening and closing of the crack exposes the newly exposed surface to the solution, which spontaneously reacts with water to form an oxide. These oxidation reactions also generate electrons which cause a further cathodic shift in the potential of the metal wire. The amount of newly exposed metal surface to the solution increases as a crack grows, thereby increasing the surface
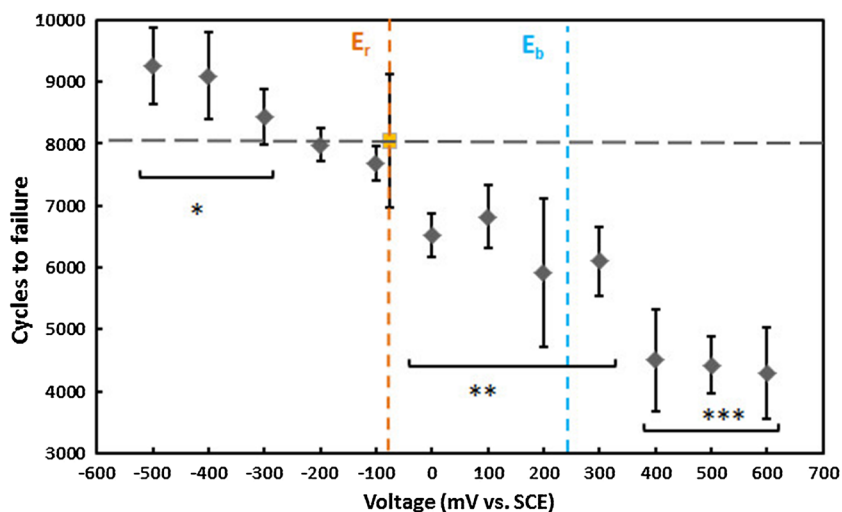
**Fig. 3** The *plot* shows the numbers of cycles to failure of an electropolished nitinol wire potentiostatically held at −500 to +600 mV (vs. SCE) while undergoing 1% alternating strain at 3600 rpm. The averages of the numbers were plotted with *error bars* representing standard deviation. The *vertical dotted lines* show where the average $E_r$ (*orange*) and $E_b$ (*blue*) lie for this material. The data point in *yellow* and the *horizontal dotted line* shows the average number of cycles to failure for wires that were tested with no applied potential (at OCP). Data points grouped by *brackets* are significantly different (Tukey pairwise comparison at $\alpha = 0.05$) from other brackets. Data point within *each bracket* is statistically similar to each other
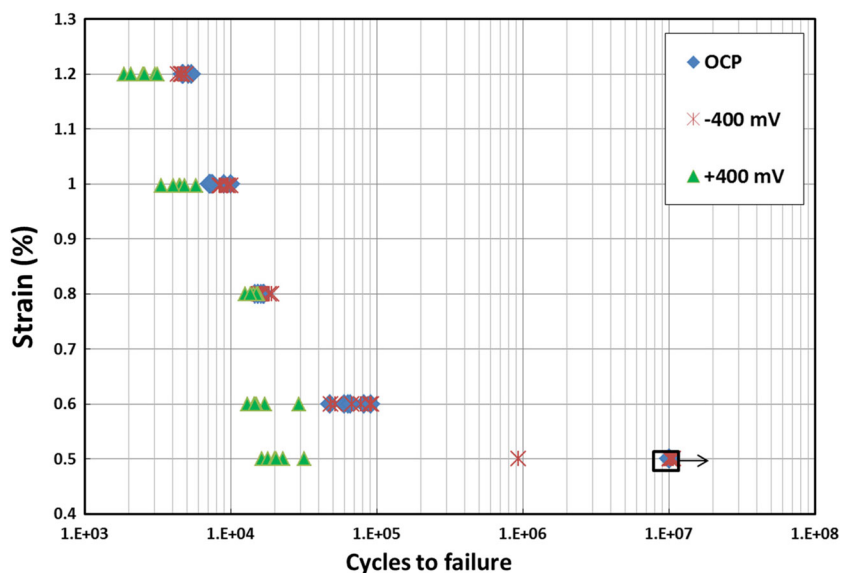


**Fig. 4** The graph shows the number of cycles to failure for different alternating strains at OCP, −400, and 400 mV (vs. SCE). Data points enclosed in a *square with arrow* denote run outs

area participating in the oxidation reaction. This is reflected in Fig. 2a where the voltage drops initially to −300 mV versus SCE and at about 100 s, the rest potential of the wire starts to gradually drop. As a crack grows with every alternating strain cycle, the rest potential gradually drops further until the crack growth evolves into the fast fracture phase. When the wire fractures, the large new metal surface is exposed to the electrolyte resulting in a sharp drop in the rest potential. Hence, the rest potential of the wire is the lowest at the event of the wire fracture. The newly formed

fracture surface will spontaneously repassivate and the rest potential will equilibrate. This is reflected in Fig. 2a where the rest potential trends in the anodic direction after fracture.

For wires that are subjected to an applied potential, the resulting current density reflects the rate of anodic or cathodic reactions occurring on the surface. The current densities reflect how the OCP of the wire would have shifted and the amount of current the potentiostat needs to supply to hold the wire to at the programmed potential. The
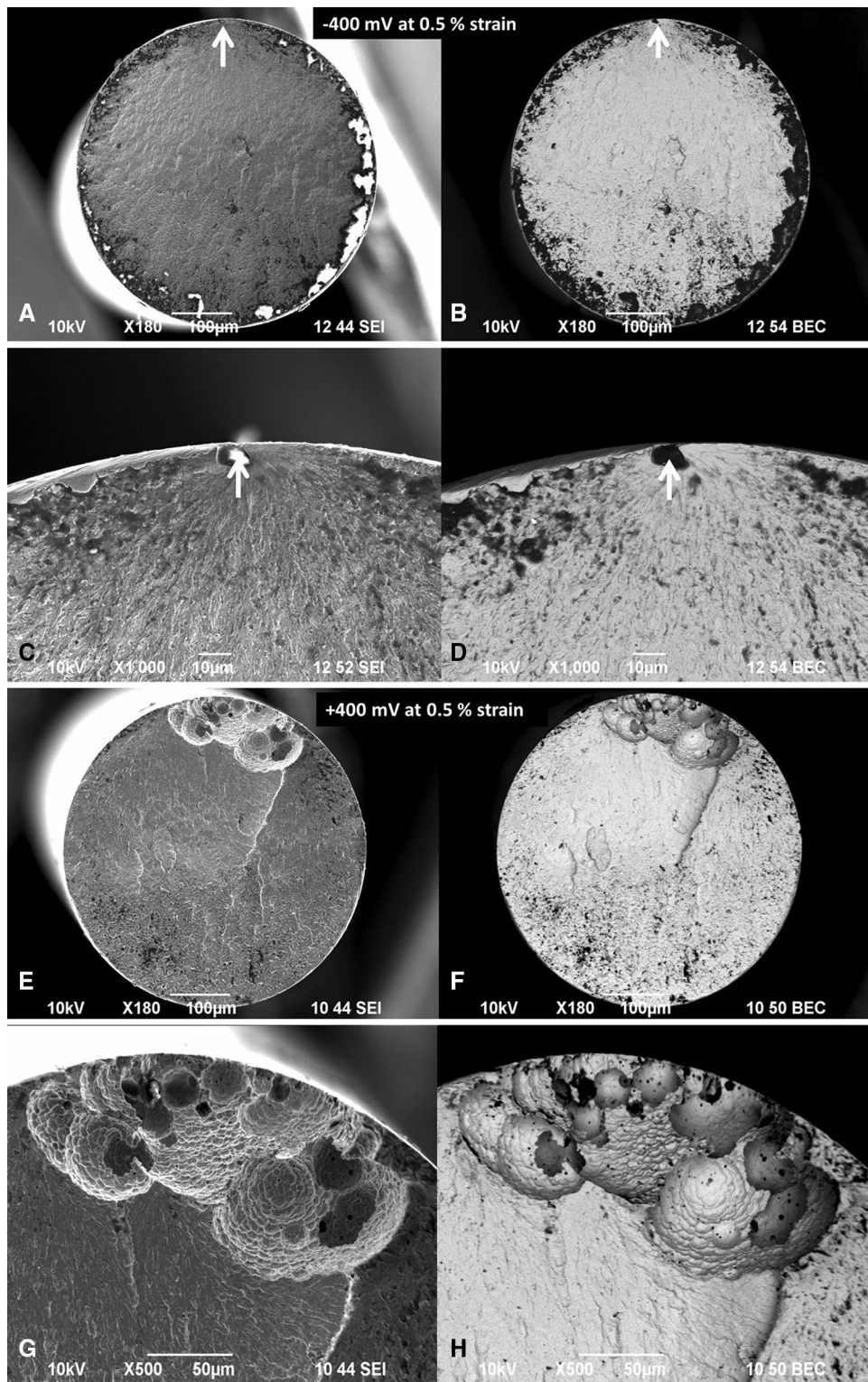
**Fig. 5** SEM micrographs **a** in secondary and **b** in backscatter of the fracture surfaces of a wire that was potentiostatically held at −400 mV versus SCE and fatigued at 0.5% strain. SEM images at high magnification in **c** secondary and **d** in backscatter show that the nucleation of the crack arose from an inclusion at the surface (*white arrow*). SEM micrographs **e** in secondary and **f** in backscatter of the fracture surfaces of a wire that was potentiostatically held at +400 mV versus SCE and fatigued at 0.5% strain. SEM images at high magnification in **g** secondary and **h** in backscatter show that the crack initiated from corrosion pits

more cathodic the applied potential from the OCP, the higher the current density the potentiostat has to supply to affix a negative potential. For the initial 10 s of the potentiostatic test, the current densities fall and stabilize quickly. When the fatigue test is initiated, there is a sharp rise in the current density. This is attributed to the disruption and repassivation of the oxide. The generation of electrons from the repassivation would have resulted in a negative shift from the rest potential. Hence, the potentiostat counters the cathodic shift by increasing the anodic currents. The current density stabilizes as the rest potential of the wire stabilizes. When new cracks nucleate and grow on the wire surface, it will cause a greater negative shift in the potential of the wire. This results in a gradual increase in anodic currents as shown in Fig. 2b, c. The current densities eventually reach the highest when the wire fails because the OCP of the wire would have been the lowest. After the wire fails, the fatigue test is stopped and the current density stabilizes and reaches equilibrium. For wire specimens that were held at a potential higher than their breakdown potential, the current densities begin to increase erratically even before the nucleation and formation of cracks. This is likely because, for potentials above the breakdown potential, some areas on the metal surface would breakdown and participate in pitting corrosion. As more metal atoms undergo oxidation and become metal ions, more electrons are generated resulting in a greater cathodic shift of the OCP. This results in the higher current density to counteract the drop in OCP to maintain the potential of the wire at +400 mV versus SCE as shown in Fig. 2d. However, we do not know if corrosion had an influence on the rate of crack growth.

SEM images of wires potentiostatically held at +400 mV in Fig. 5 show the formation and propagation of the crack which occurs away from the surface of the wire that underwent pitting. The images also show that the pits formed from the breakdown of the wire were spheroidal in shape and were subsurface in nature. The pits were interconnected and filled with corrosion byproducts. The fracture surface shows that the fatigue striations were observed to have different directions which may be a result of the evolution of new cracks resulting from new stress concentration points from the active pitting occurring on the metal surface. In contrast, wires that were potentiostatically held at −400 mV (Fig. 5a, b) did not have corrosion pits on the surface of the wires and crack nucleation sites tended to be associated with non-metallic inclusions.

Wires that were held at potentials lower than the metal's breakdown potential had a higher number of cycles to failure compared to those wires held at potentials above the breakdown for all levels of strain. At potentials below the rest potential, the repassivation of the oxide layer would be suppressed and this could have an influence on the

chemistry of the solution within the crack. In Fig. 3, the graph shows that wires that were potentiostatically held at −400 mV survived for a high number of cycles when compared to the wires that were held at 100 mV. The relative location of the average breakdown potential (dotted blue line) to the rest potential, $E_r$ (dotted orange line) gives us an indication of the corrosion susceptibility of the tested wires. The horizontal dotted gray line shows us the average number of cycles that was needed for failure of the wire when no potential was enforced. This helps us compare the average number of cycles to failure for each potential to those that failed when no voltage was enforced, that is, at OCP. The fatigue performance of the wires at OCP is characteristic of material with a relatively high upper plateau stress (see Table 1.). The $E_b$ and $E_r$ are values that were obtained from ASTM F2129 testing performed in deaerated PBS while the fatigue tests were done in PBS without de-aeration. This may explain why the drop in fatigue life occurs between +300 and +400 mV versus SCE rather than at $E_b$. The breakdown potential will be higher in aerated PBS [16] and this may have shifted the $E_b$ closer to +400 mV for our fatigue test conditions. However, Fig. 4 shows that the number of cycles to failure for the wires fatigued at −400 mV was similar to those that were fatigued at OCP except for 1.2% strain. This is because the open circuit potential for a wire that is undergoing fatigue will become cathodic rather than continue to remain at the baseline rest potential. Hence, the number of cycles required for failure for wires at −400 mV was similar to those for which no potential was enforced. The impact of positive potentials on fatigue life was more pronounced at lower levels of strain. Here, the applied potential and the alternating strain can have a synergistic effect to decrease the time required to cause wire fracture as shown in Fig. 4. For example, wires that were subjected to alternating strain 0.5% at +400 mV versus SCE took an average of 21,637 cycles to cause wire fracture. Whereas five out of six wires that were held to potentials cathodic to the breakdown potential, −400 mV versus SCE, were run outs and one failed approximately at 900,000 cycles. This implies that the effect of positive potential on the fatigue life is more pronounced at lower strain levels when compared to those tested at higher strain levels. Similarly, all six wires that were at OCP and at 0.5% strain were run outs.

To demonstrate that the rise in current densities (in potentiostatic experiments) precedes the event of wire fracture, one wire was held potentiostatically at +100 mV versus SCE and subjected to fatigue. The test was stopped when the gradual rise in current density was observed and just prior to wire fracture. Figure 6 shows paired SEM images for this wire where some fatigue-initiated cracks were found to traverse the circumference of the wire. The
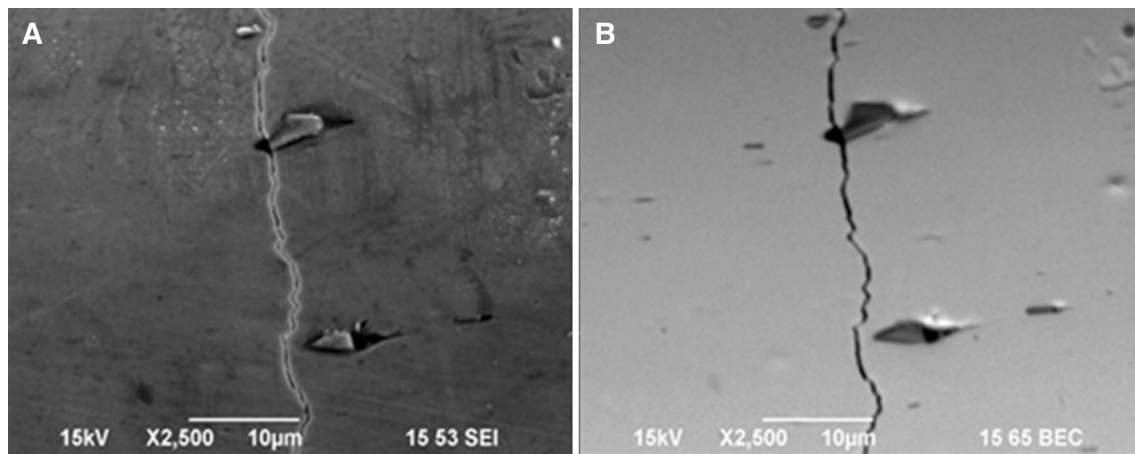
**Fig. 6** Paired scanning electron micrographs in **a** secondary and **b** in backscatter, show a crack initiating from the surface inclusion (precipitates) on a wire that was subjected to alternating 1% strain. A wire was potentiostatically held at +100 mV versus SCE and fatigued until a gradual increase in current density was observed. The fatigue test was stopped before wire failure and imaged using SEM. *Note* the inclusions appear as dark islands on the backscatter image

figure also shows that the crack goes through the interface between the inclusion and void on the surface of the wires, which may have played a role in the time to initiate a fracture. The inclusions appear dark in the backscatter image since their compositions have a lower atomic number when compared to the surrounding microstructure. This drop in OCP preceding the fracture of the wire is similar to what was reported by Neelakantan et al. [23]. Therefore, these electrochemical techniques could be used to detect and monitor fatigue damage on specimens being tested, specifically to better detect crack initiation and growth.

This study also shows that the fatigue life at 1% $\varepsilon_a$ improved (Fig. 3) for wires held at potentials very cathodic to the rest potential when compared to fatigue life of wires held in-between $E_r$ and $E_b$. This could be attributed to the suppressed oxidation reaction at cathodic potentials, where limiting the oxidation reactions on the bare nitinol surface would result in suppressing the formation of the oxide within the newly formed crack. A recent study by Racek et al. [19] has shown that the confined geometry and chemistry within the newly formed crack on nitinol would result in the formation of a hydrated titanium oxide which would suppress the diffusion of hydrogen into the bulk solution. This would cause the hydrogen to diffuse into the metal surface and cause hydrogen embrittlement of the microstructure. Racek et al. showed that this results in the formation of hydrogen traps within the crack geometry. This may explain why at cathodic potentials the fatigue life at 1% $\varepsilon_a$ is improved for these wires because at these potentials hydrogen formation is also suppressed which in turn suppresses hydrogen embrittlement within the crack geometry. In Fig. 3, the fatigue life of wires (for $\varepsilon_a = 1\%$) that were at potentials in-between the rest and breakdown potentials were found to be statistically similar. This could

imply that hydrogen embrittlement and the formation of hydrogen traps at the tip of the growing crack were not suppressed between $E_r$ and $E_b$. However, in this study, we have not investigated the formation of the hydrogen traps or their absence thereof at the different applied potentials.

More interestingly, as shown in Fig. 4, at most alternating strains, the fatigue life of wires held at −400 mV was not significantly different from wires that were fatigued at OCP. Although there was a statistically significant difference in fatigue life at 1.2% $\varepsilon_a$ for −400 mV and OCP, the actual magnitude of this difference is in line with expectations of variability for this kind of test [21]. Overall, the improvement in fatigue life was only observed at 1% $\varepsilon_a$ for wires held at very cathodic potentials when compared to those wires that were held between $E_r$ and $E_b$. This improvement was not observed when we compared wires held at −400 mV and OCP (as seen in Fig. 4). This may be because when wires were fatigued with no potential applied (at OCP), the rest potential of the wire would naturally drop to cathodic potentials as a result of repassivation reactions as shown in Fig. 2a.

While this study shows that the potential of the wire will have an effect on its fatigue life, we do not yet know how long these deviations from the OCP of the metal surface would occur in vivo. For example, for overlapping stents, different struts may come in and out of contact as the stents experience mechanical strains. The negative drop in potential resulting from fretting may last from a few milliseconds to a few seconds and whether this period is sufficient enough to have an influence on the fatigue life of the device is yet to be determined. Other deleterious consequences of fretting such as generation of wear debris, toxic metal ions from fretting-associated corrosion may play a larger role in contributing towards the failure of the

device. However, the effect of inflammatory reactions occurring around the implant will cause the potential of the device to deviate from OCP [15] to more positive potentials (up to +500 mV for CoCrMo) for longer time periods and this could have an impact on its fatigue life. This is because the change in pH of the local environment due to a chronic inflammatory reaction will last from days to weeks [24]. While this study investigated the effect of potential on fatigue life of electropolished nitinol, the effect of applied potential on wires made from other metal alloys might be different. The effect on fatigue life will depend on the electrochemical properties such as the rest potential and the breakdown potential. Metals that do not have a breakdown potential may be less susceptible to the combined effects of applied potential and strain. For example, metal alloys such as MP35N used in pacemaker leads do not typically undergo breakdown via pitting corrosion, but corrode at anodic potentials via etching of the grain boundaries or via transpassive dissolution [25]. Whether the applied potential would have an effect on the fatigue life of MP35N or other similar materials is yet to be determined. The result of this study gives us an insight into how an applied potential can influence the fatigue life of nitinol wires. For active cardiovascular devices such as insulated leads, failure of the insulation could expose the active metal surface to the physiological environment and make the surface prone to corrosion and reduced durability. As for devices such as stents and endografts, the voltage at the metal surface could be used to simulate test conditions that mimic inflammatory reactions or the presence of fretting while evaluating its durability. This is important because most of the testing done currently assume that there are no inflammatory reactions or fretting occurring on the implant surface. Voltage excursions away from breakdown potential to more anodic potentials under inflammatory conditions could have a negative impact on the fatigue life and ultimately affect the clinical performance of medical devices.

## Conclusion

This study showed that applied potential can influence the fatigue life of nitinol wire. Fracture initiation at cathodic potentials was due to surface defects already present on the surface of the wire. Whereas, at potentials anodic to the breakdown potential, the formation of new pits from corrosion occurring on the metal surface acted as stress concentrators that led to the formation of a fatigue crack. Further work needs to be done to understand how applied potentials would affect the fatigue life of wires made from other metal alloys and also to better understand the in vivo environment.

## References

1. Duerig T, Tolomeo D, Wholey M (2000) An overview of superelastic stent design. Minim Invasive Ther Allied Technol 9(3–4):235–246
2. Adlakha S, Sheikh M, Wu J, Burket MW, Pandya U, Colyer W, Eltahawy E, Cooper CJ (2010) Stent fracture in the coronary and peripheral arteries. J Interv Cardiol 23(4):411–419
3. Chakravarty T, White AJ, Buch M, Naik H, Doctor N, Schapira J, Kar S, Forrester JS, Weiss RE, Makkar R (2010) Meta-analysis of incidence, clinical characteristics and implications of stent fracture. Am J Cardiol 106(8):1075–1080
4. Haas A (2007) The phagosome: compartment with a license to kill. Traffic 8(4):311–330
5. Shabalovskaya SA, Anderegg JW, Undisz A, Rettenmayr M, Rondelli GC (2012) Corrosion resistance, chemistry, and mechanical aspects of nitinol surfaces formed in hydrogen peroxide solutions. J Biomed Mater Res B Appl Biomater 100(6):1490–1499
6. Swaminathan V, Gilbert JL (2012) Fretting corrosion of CoCrMo and Ti6Al4 V interfaces. Biomaterials 33(22):5487–5503
7. Wazni O, Wilkoff BL (2016) Considerations for cardiac device lead extraction. Nat Rev Cardiol 13(4):221–229
8. Nichols CI, Vose JG, Mittal S (2016) Incidence and costs related to lead damage occurring within the first year after a cardiac implantable electronic device replacement procedure. J Am Heart Assoc 5(2):e002813
9. Shah AD, Hirsh DS, Langberg JJ (2016) Sudden and fatal malfunction of a durata defibrillator lead due to external insulation failure. Pacing Clin Electrophysiol 39(1):101–104
10. Lim KK, Reddy S, Desai S, Smelley M, Kim SS, Beshai JF, Lin AC, Burke MC, Knight BP (2009) Effects of electrocautery on transvenous lead insulation materials. J Cardiovasc Electrophysiol 20(4):429–435
11. Eng LK, Walters TE, Gould PA (2012) Implantable cardioverter-defibrillator failure unmasked by a "lucky" shock. J Arrhythm 28(4):254–257
12. Hauser RG, McGriff D, Retel LK (2012) Riata implantable cardioverter-defibrillator lead failure: analysis of explanted leads with a unique insulation defect. Heart Rhythm 9(5):742–749
13. Kanemura T, Yokoyama KI, Sakai JI (2008) Effects of acid type on corrosion and fracture behavior of Ni–Ti superelastic alloy under sustained tensile load in physiological saline solution containing hydrogen peroxide. Corros Sci 50(10):2785–2795
14. Yokoyama KI, Ogawa T, Fujita A, Asaoka K, Sakai JI (2007) Fracture of Ni-Ti superelastic alloy under sustained tensile load in physiological saline solution containing hydrogen peroxide. J Biomed Mater Res Part A 82(3):558–567
15. Gilbert JL, Sivan S, Liu Y, Kocagöz SB, Arnholt CM, Kurtz SM (2015) Direct in vivo inflammatory cell-induced corrosion of CoCrMo alloy orthopedic implant surfaces. J Biomed Mater Res Part A 103(1):211–223
16. Lonn MK, Metcalf JM, Choules BD (2015) In vivo and in vitro nitinol corrosion properties. Shape Mem Superelasticity 1(3):328–338

17. Ehrensberger MT, Gilbert JL (2010) The effect of static applied potential on the 24-hour impedance behavior of commercially pure titanium in simulated biological conditions. J Biomed Mater Res B Appl Biomater 93(1):106–112

18. Sullivan SJ, Dreher ML, Zheng J, Chen L, Madamba D, Miyashiro K, Trépanier C, Nagaraja S (2015) Effects of oxide layer composition and radial compression on nickel release in nitinol stents. Shape Mem Superelasticity 1(3):319–327

19. Racek J, Stora M, Šittner P, Heller L, Kopeček J, Petrenec M (2015) Monitoring tensile fatigue of superelastic NiTi wire in liquids by electrochemical potential. Shape Mem Superelasticity 1(2):204–230

20. ASTM-F2129-15 (2015) Standard test method for conducting cyclic potentiodynamic polarization measurements to determine the corrosion susceptibility of small implant devices. ASTM International, West Conshohocken

21. ASTM-E2948-16a (2016) Standard test method for conducting rotating bending fatigue test of solid round fine wire. ASTM International, West Conshohocken

22. Di Prima M, Gutierrez E, Weaver JD (2016) The effect of fatigue on the corrosion resistance of common medical alloys. J Biomed Mater Res Part B. doi:10.1002/jbm.b.33738

23. Neelakantan L, Zglinski JK, Frotscher M, Eggeler G (2013) Design and fabrication of a bending rotation fatigue test rig for in situ electrochemical analysis during fatigue testing of NiTi shape memory alloy wires. Rev Sci Instrum 84(3):035102

24. Farb A, Sangiorgi G, Carter AJ, Walley VM, Edwards WD, Schwartz RS, Virmani R (1999) Pathology of acute and chronic coronary stenting in humans. Circulation 99(1):44–52

25. Pound BG (2010) Electrochemical behavior of cobalt–chromium alloys in a simulated physiological solution. J Biomed Mater Res Part A 94A(1):93–102